



Lake Ice Thickness

D4-2: Product generation, uncertainty measure, quality flags, and validation

Reference: CCI-LAKES-0078-PVIR

Issue: 1.1

Date: 27 June-2022

Version history:			
Issue:	Date:	Reason for change:	Author
1.0	24 June-2022	Initial Version	C. Duguay et al.
1.1	27 June 2022	Revision following ESA review	C. Duguay et al.

People involved in this issue:			Signature
Authors:	Claude Duguay	H2O Geomatics	
	Anna Mangilli Pierre Thibaut	CLS	
	Elena Zakharova	Eola	
	Alexei Kouraev	LEGOS	
Internal review:	Stefan Simis	Plymouth Marine Laboratory	
Approved by:	Bruno Coulon	CLS	
Authorized by:	Clément Albergel	ESA	

Distribution:		
Company	Names	Contact Details
ESA	C. Albergel	Clement.Albergel@esa.int
CLS	B. Coulon B. Calmettes A. Mangilli P. Thibaut	bcoulon@groupcls.com bcalmettes@groupcls.com amangilli@groupcls.com pthibaut@groupcls.com
Eola	E. Zakharova	zavocado@gmail.com
H2OG	C. Duguay	claude.duguay@h2ogeomatics.com
LEGOS	J.F. Crétaux A. Kouraev	jean.francois.cretaux@legos.obs-mip.fr kouraev@legos.obs-mip.fr
PML	S. Simis	stsi@pml.ac.uk

List of Contents

1. Summary5

2. Introduction6

3. Product Generation Based on LRM Radar Waveforms and Validation (CLS)7

 3.1. *Product Generation* 7

 3.2. *Product content, quality assessment and validation* 8

 3.2.1. Product content 8

 3.2.2. Region of Interest (RoI) of the LIT analysis..... 9

 3.2.3. LIT retrieval 9

 3.2.4. LIT uncertainty and quality flag..... 10

 3.2.5. Validation 12

 3.3. *Conclusions*..... 15

4. Product Generation Based on Backscatter/Brightness Temperature and Validation (EOLA/LEGOS)16

 4.1. *Product Generation* 17

 4.1.1. Input Data 17

 4.1.2. Method..... 17

 4.2. *Validation* 18

 4.3. *Conclusion and Recommendations* 22

5. Comparison of LIT Retrievals from Radar Waveforms and Backscatter/Brightness Temperature Approaches25

6. References27

1. Summary

This document provides a description of lake ice thickness (LIT) product generation from two distinct retrieval approaches and complements D4-1 (Ice thickness dataset with included uncertainty measure and quality flags). The first (analytical) approach, developed at CLS, is a retracker specific to LIT analysis based on the physical modelling of Low Resolution Mode (LRM) radar waveforms. The second approach, developed by Eola/LEGOS, is an empirical one that requires the development of lake-specific statistical relations (regression-type equations) between backscatter/brightness temperature and LIT obtained from a numerical lake ice model (or in-situ measurements where available) for calibration. Some of the limitations of each approach and recommendations for improvement of the empirical approach are provided. The document also presents results from the validation of products generated from both approaches and their comparison using Jason-2 data acquired at Great Slave Lake, Canada over three overlapping ice seasons (2013-2016).

2. Introduction

Two distinct approaches (algorithms) have been developed for the retrieval of lake ice thickness (LIT) using Low Resolution Mode (LRM) data from altimetry missions. This document provides a description of how LIT products are generated based on the approaches developed at CLS and Eola/LEGOS as well as the validation of products and their comparison. Associated LIT products have been delivered under D4-1 (Ice thickness dataset with included uncertainty measure and quality flags). Details regarding the retrieval algorithms and their implementation can be found in D2 (Technical Note: Algorithm Theoretical Basis Document (ATBD)) and D3 (Short system development document describing the processing implemented at CLS and LEGOS), respectively.

3. Product Generation Based on LRM Radar Waveforms and Validation (CLS)

This section summarizes the LIT product generation with the algorithm based on LRM radar waveforms (LRM_LIT retracking algorithm). Details of the algorithm and its validation can be found in Mangilli et al. (2022).

3.1. Product Generation

The LIT product is generated using the LRM_LIT algorithm (Mangilli et al., 2022), a retracker specific to the LIT analysis based on the physical modelling of the LRM radar waveforms. For each data cycle, and a given Region Of Interest (ROI) defined by a latitude cut $LW_{LIT} = [lat_{min}, lat_{max}]$ over a given target lake, the LIT product generation consists of the following steps: 1) the optimization step, that is, the waveform fit, 2) the data editing and estimation of the LIT mean and standard deviation, and 3) the quality flag computation, as described below.

Step 1: Optimisation and best fit parameters

The optimisation step consists of performing a Least Square Levenberg-Marquardt weighted fit of each echo in the LIT analysis window with the LRM_LIT model described in Mangilli et al. (2022). The optimized function is chi-squared function:

$$\chi^2 = \mathbf{r}^T \mathbf{C}^{-1} \mathbf{r} \simeq \sum_i \left(\frac{r_i}{\sigma_i} \right)^2 \quad (1)$$

where, $\mathbf{r} = \mathbf{y}(x) - S_{\text{model}}(x; \theta_p)$ is the vector of residuals between the waveform data, $\mathbf{y}(x)$, and the model, $S_{\text{model}}(x; \theta_p)$. The weights, σ_i , are computed as the standard deviation of the echoes within the LIT ROI analysis window. For each data cycle, a set of best fit values for each of the 5 parameters, including the LIT, is provided from the fit of the individuals echos in the analysis window. The value of the reduced chi2 statistics, that is, the chi-squared function at the best fit divided by the number of degrees of freedom is also computed:

$$\hat{\chi}^2 = \frac{1}{\nu} \chi^2(\bar{\theta}_p) \quad (2)$$

where ν is the number of degrees of freedom, that is the number of observations minus the number of fitted parameters, and $\chi^2(\bar{\theta}_p)$ is the minimum of the optimized function. If the weights are representative of the data set, a reduced chi2 of order 1 is expected for a fit performing correctly, indicating that the data and the model are in agreement within the variance.

Step 2: Data editing and parameter estimation for LIT retrieval

The second step of the retracking analysis is the parameters estimation, which provides, as the main output, the LIT measurement with the associated uncertainty. The estimation is done by computing the mean and standard deviation of the best fit parameters for each data cycle in the LIT ROI analysis window. In order to manage eventual outliers, fit results for which the model and the observations are in agreement within three standard deviations, that is a reduced chi2 < 3, are selected. Also, a threshold is set to discard the fit results that could provide an unrealistic LIT value of $LIT > 3$ m and the final histograms are built considering the LIT estimates up to 2 std around the mean. The std is set to 0.25 m, so that LIT estimates within a window of 1 m around the mean are taken into account for the LIT analysis. This is a conservative choice considering that maximum LIT values within an ice season rarely exceed 1.5 m. Finally, a Gaussian fit on the outliers-cut histograms, obtained with the data editing procedure described above, provides the mean and variance for each parameter. The LIT estimates (LIT mean and std in the ROI) and the median of the reduced chi-2 statistics in the ROI are stored in the LIT product.

Step 3: LIT quality flag

A quality flag is added to the LIT product. This flag can take three values as follows:

- LIT_flag = 0 : good LIT data
- LIT_flag = 1 : bad data (no or bad input data. The LIT analysis could not be performed)

LIT_flag = 2 : degraded fit performances with reduced $\chi^2 > 2.5$ (but < 3 by definition). The LIT measurements can be used but the fit performances are degraded. This indicates difficulty of retracking specific region/periods and typically happens at the seasonal transitions, especially during melting season.

3.2. Product content, quality assessment and validation

This section summarizes the LIT product content and provides an illustrative example based on the delivered D4-1 dataset. The D4-1 dataset consists of a LIT time series over the Great Slave Lake (Canada) for the 2013-2016 period, obtained using Jason-2 data. This dataset has been validated using CLIMO simulations (Duguay et al., 2003) and is qualitatively in agreement with in situ data. It is worth mentioning that a quantitative comparison and validation with in-situ data is not possible as in-situ data are collected in Back Bay near Yellowknife, while Jason data are taken from a track in the middle of the lake (see Figure 1). These are indeed two different environments in terms of bathymetry, wind exposure, snow type and quantity. All these parameters play a key role on ice formation and thickness, and they can lead to LIT differences in the order of tens of centimeters. Details on the validation can be found in Mangilli et al. (2022).

3.2.1. Product content

The structure of LIT output product from the radar waveform method (LRM_LIT retracker) is presented in Table 1. Data are provided in NetCDF format.

Table 1. List of variables of the LRM_LIT retracker product.

Variable name	Description	Units	Dims
time	Time of measurement	UTC seconds since 1970	time
lon	Longitude of the center of the Region of Interest on which the LIT measurement is done [-180;+180]	degrees	time
lat	Latitude of the center of the Region of Interest on which the LIT measurement is done. [-90;+90]	degrees	time
LIT	Ice thickness retrieved from the radar waveform method (LRM_LIT retracker) [0; 3]	m	time
LIT_std	Standard deviation of Lake Ice thickness retrieved with the radar waveform method	m	time
Flag_qual_LIT	LIT quality flag [0:good; 1:no or bad data; 2:measurement can be used but the fit quality is degraded (median of the reduced χ^2 values in the $2.5 < \text{ROI} < 3$)]		time
red_chi2_fit	Median of the reduced χ^2 statistics of the LRM_LIT retracker fit in the ROI [0,3]		

Global Attributes	Description
mission	Satellite mission name
lake_id	Lake ID (as in the CCI-LAKES database)

3.2.2. Region of Interest (RoI) of the LIT analysis

The RoI of the LIT analysis used for the D4-1 dataset is a segment of Jason-2 pass 45 over GSL, illustrated by the green segment in Figure 1. The product contains the longitude and latitude coordinates of the center of the RoI used for the LIT analysis. The RoI covers ~ 0.2 degrees in latitude around the center.

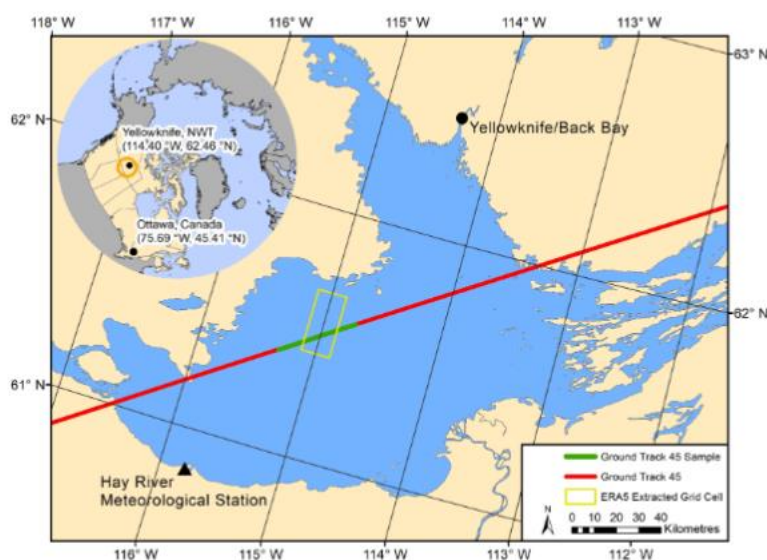


Figure 1. Jason-2 overpass track 45 over Great Slave Lake (red). The section of the track used for the baseline LIT analysis is shown in green. The location of Back Bay, near Yellowknife (Northwest Territories, Canada), where weekly ice thickness measurements are available is also shown. Source: Mangilli et al. (2022).

3.2.3. LIT retrieval

The product contains the LIT mean (variable name in the product: LIT) obtained with the LRM_LIT retracker in the RoI. LIT measurements are taken from December to May of each year.

An example of the evolution of the LIT retrieval over the three ice seasons in D4-1 is shown in Figure 2. The seasonal transitions (ice forming and melting) and inter-seasonal LIT variations are clearly visible.

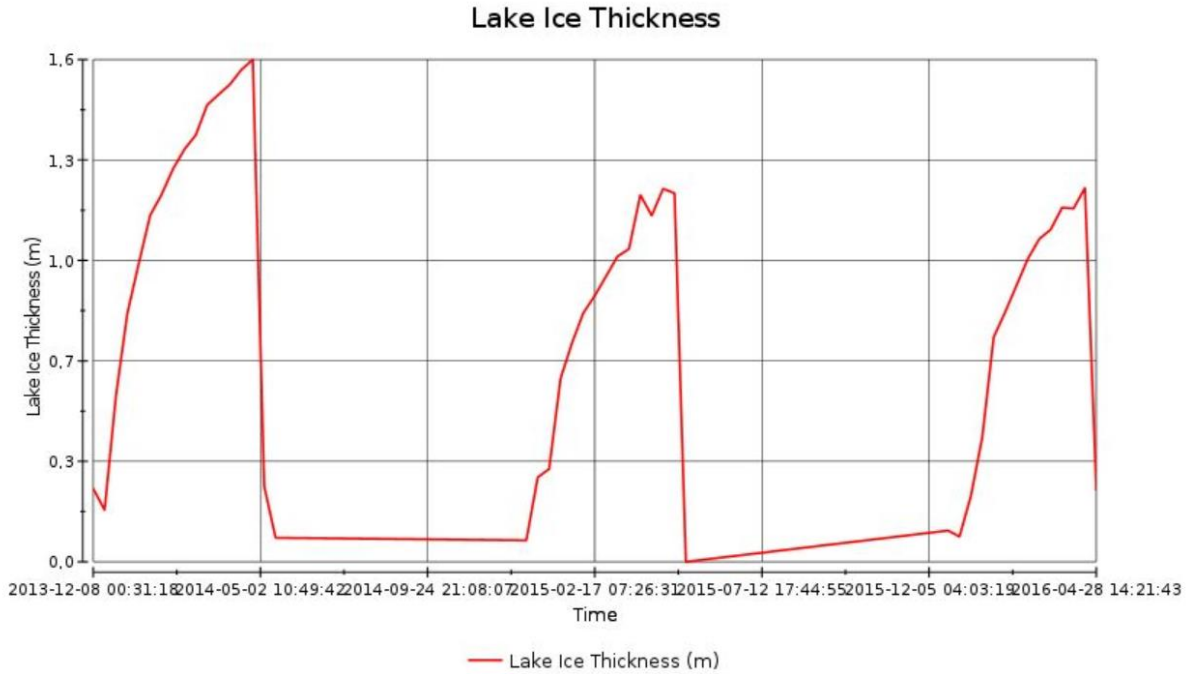


Figure 2. Evolution of the LIT at Great Slave Lake over three ice seasons (2013-2014, 2014-2015, and 2015-2016).

3.2.4. LIT uncertainty and quality flag

The LIT product contains the uncertainty of the LIT measurements in the RoI (LIT standard deviation, variable: LIT_std). An example of the evolution of the accuracy of the LIT estimates over the three ice seasons is given in Figure 3.

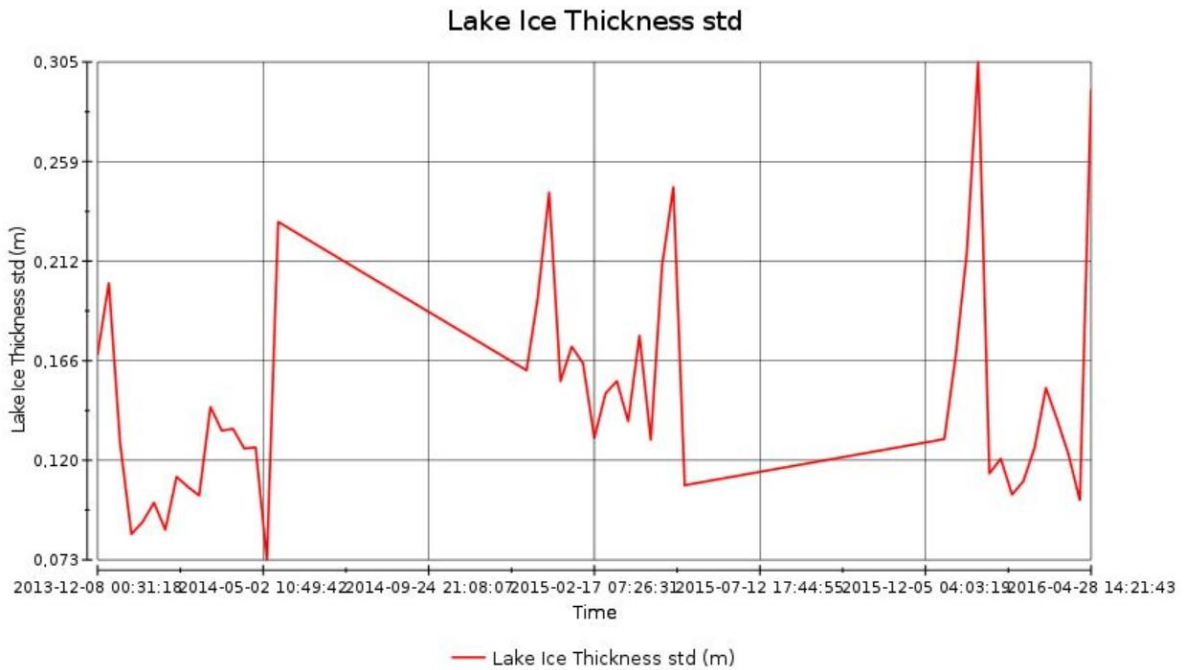


Figure 3. Evolution of the accuracy of the LIT estimates at Great Slave Lake over three ice seasons (2013-2014, 2014-2015, and 2015-2016).

In the middle of the ice seasons, when the ice is well established, the LIT uncertainty is of the order of 10 cm. At the seasonal transitions, the uncertainty of the LIT measurements is increased by about a factor of 2, because the lake surface in RoI is not homogeneous, which results in a greater spatial variability of the LIT measurements (greater variance in the RoI).

The product contains the median of the reduced chi2 statistics in the RoI (variable: red_chi2_fit) and the quality flag (variable: flag_qual_LIT). In the reduced chi2 plot (Figure 4), the fit performance degradation, in particular during the melt season, is visible. While the fit still performs correctly, the reduced chi2 increases, with values around or greater of 2, indicating the difficulty in retracking an irregular and reflective surface.

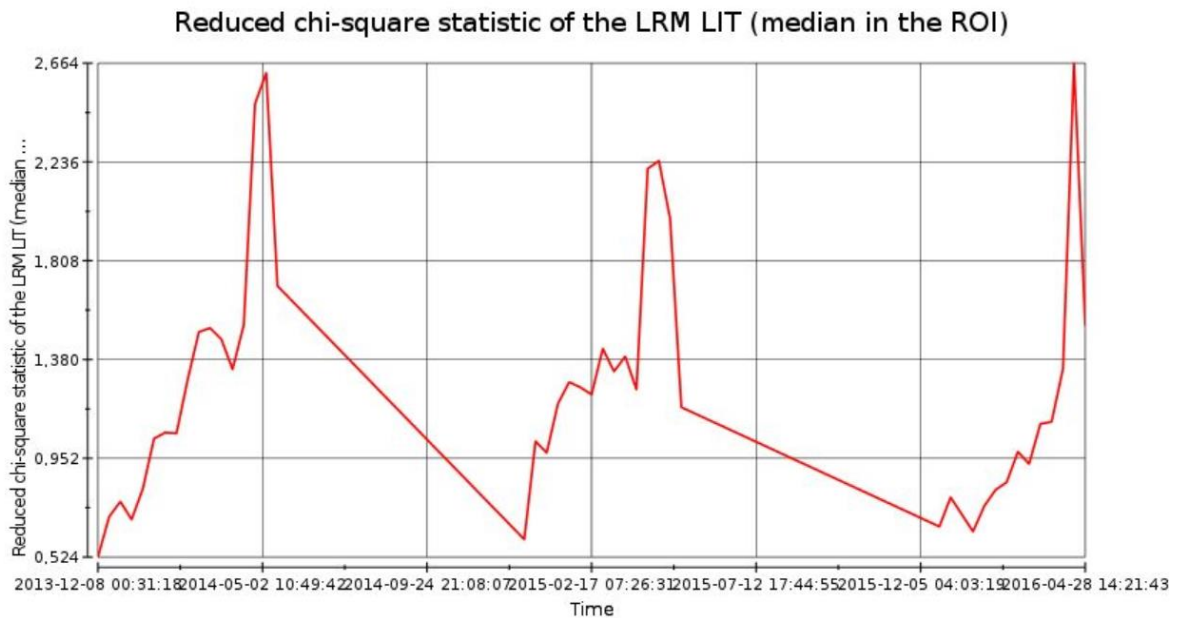


Figure 4. Evolution of chi2 of the LIT estimates at Great Slave Lake over three ice seasons (2013-2014, 2014-2015, and 2015-2016).

The quality flag (Figure 5) is set to 0 for good LIT data, to 1 for bad data (bad or not available input data) and to 2 when the median of the reduced chi2 values in the RoI is > 2.5 . Flag values at 2 indicates that the fit performances are degraded. In the examples this happen at the melting season reflecting again the difficulty in retracking an irregular and reflective surface. Yet, the LIT data can be used as the fit still performs correctly. Because of the data editing, fits with very low performances with red chi2 > 3 are not included in the final LIT estimates used to generate the product.

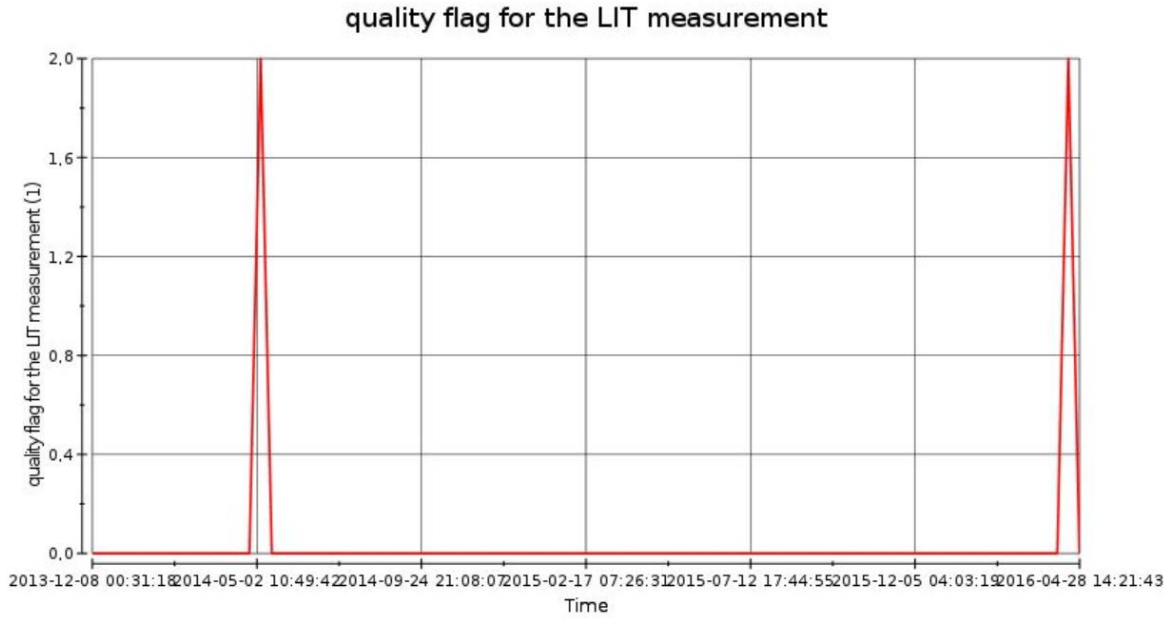


Figure 5. Evolution of the quality flag of LIT estimates at Great Slave Lake over three ice seasons (2013-2014, 2014-2015, and 2015-2016).

3.2.5. Validation

The figures below summarize the validation of the LIT results of the D4-1 product as described in detail in Mangilli et al. (2022).

Figure 6 shows the evolution of Jason-2 LIT estimates over Great Slave Lake along track 45 for WS3 (winter season 2015-2016). Plots in the left column show, from top to bottom, along-track Jason-2 LIT estimates superimposed on MODIS/RADARSAT-2 images on the same date or within one day in December, February, March and end of April. Plots in the right column show the evolution of the Jason-2 LIT estimates as a function of latitude (top plots) and of the reduced chi-squared statistics as a function of the latitude (bottom plots) along the track.

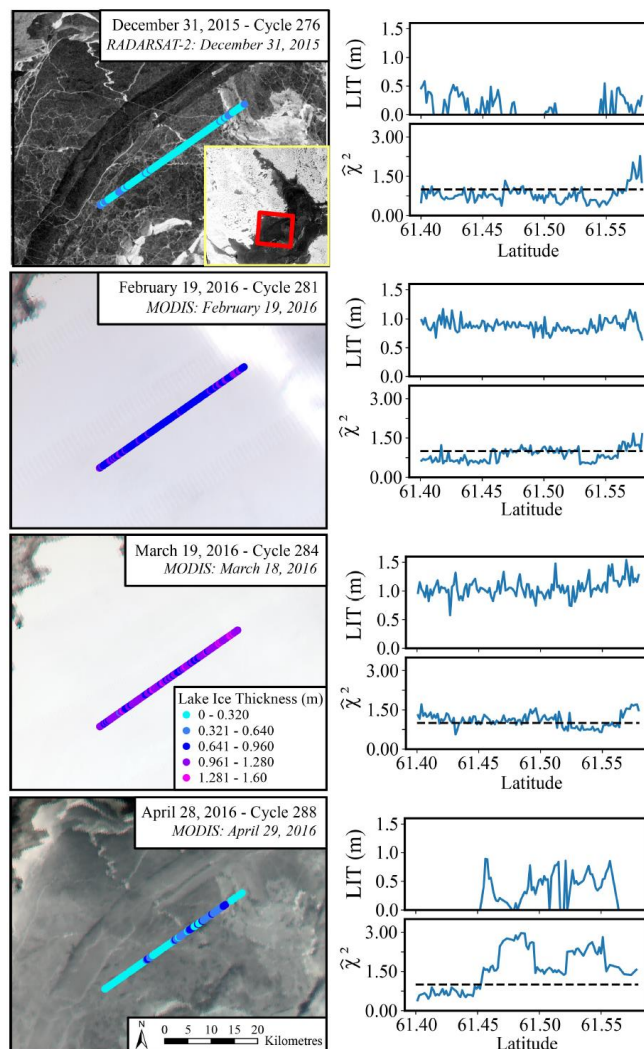


Figure 6. Evolution of Jason-2 LIT estimates over Great Slave Lake along track 45 for WS3 (winter season 2015-2016). Plots in the left column show, from top to bottom, along-track Jason-2 LIT estimates superimposed on MODIS images on the same date or within one day in December, February, March and end of April. Plots in the right column show the evolution of the Jason-2 LIT estimates as a function of latitude (top plots) and of the reduced chi-squared statistics as a function of the latitude (bottom plots) along the track. Source: Mangilli et al. (2022).

As it can be seen from the image in the top left, in December, at the beginning of the ice season, ice has begun to form but the ice cover over the selected region is not homogeneous, with parts of the lake that have already frozen and others where the ice is thin with cracks in the vicinity of the track (dark area to the north in RADARSAT-2 image). LIT estimates as a function of latitude, shown in the top right plot, are overall compatible with zero with values ranging from 0 to 0.5 m; the fit performs slightly worse with some reduced χ^2 values greater than 2 due to the difficulties of retracing the radar waveforms over an irregular and heterogeneous surface. In the middle of the ice season, typically from February to mid-April, when the ice is well established, the ice (and overlaying snow) cover is relatively homogeneous, as shown in MODIS images of the second and third row. The fit performs well for all the waveforms in the analysis window, yielding reduced χ^2 results all close to a value of one and consistent LIT estimates with ice growth. At the end of the season (last row of the figure), the ice cover is also irregular. The MODIS image of late April, which is characterized by lower reflectance than in the previous dates, indeed indicates that the melt season is underway. In particular, the image reveals that the snow cover has largely melted from the ice surface which translates into low reflectance in the area of the Jason-2 track. The LIT fit yields consistent results, yet with some regions exhibiting slightly increased reduced χ^2 due to the difficulty in retracing an

irregular and reflective surface. Overall, the LIT estimates are fully consistent with what is expected and seen in the RADARSAT-2/MODIS images.

Figure 7 shows the LIT estimates over Great Slave Lake for the three winter seasons: WS1 2013-2014 (top), WS2 2014-2015 (middle), and WS3 2015-2016 (bottom). Shown are a comparison between LIT estimates with the LRM_LIT retracker from Jason-2 (triangles) and Jason-3 (stars) data, CLIMo simulations (diamonds) and in situ data (circles). The shaded areas correspond to the LIT estimation uncertainties computed from Jason-2 data (blue) and Jason-3 data (red). Three different realizations of CLIMo simulations are shown by varying the amount of snow on the ice surface. The in situ data consist of ice thickness measurements collected in Back Bay near Yellowknife. Overall, these results demonstrate that LIT estimates can be retrieved from radar altimetry data that are compatible with thermodynamic simulations and qualitatively in agreement with in situ measurements.

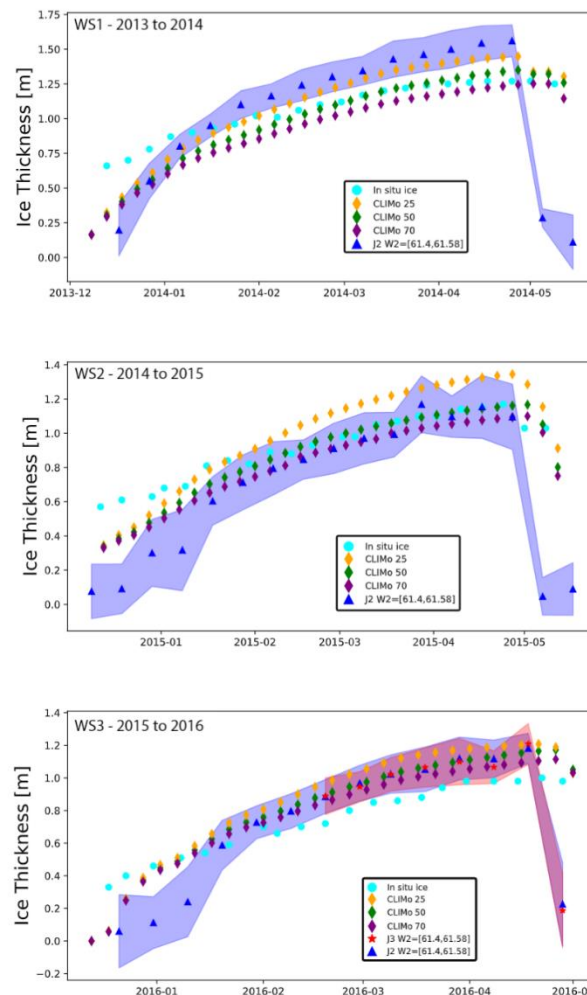


Figure 7. LIT estimates over Great Slave Lake for three winter seasons: WS1 2013-2014 (top), WS2 2014-2015 (middle), and WS3 2015-2016 (bottom). Shown are a comparison between LIT estimates with the LRM_LIT retracker from Jason-2 (triangles) and Jason-3 (stars) data, CLIMo simulations (diamonds) and in situ data (circles). The shaded areas correspond to the LIT estimation uncertainties computed from Jason-2 data (blue) and Jason-3 data (red). Three different realizations of CLIMo simulations are shown by varying the amount of snow on the ice surface. The in situ data consist of ice thickness measurements collected in Back Bay near Yellowknife. Source: Mangilli et al. (2022).

3.3. Conclusions

This section presented an illustrative example of LIT analysis and product obtained by using the LRM_LIT retracker method. The LIT analysis was performed over one representative lake, Great Slave Lake, but the method can be easily generalized to other target lakes providing that the ice signature, that is, the step like feature in the leading edge, is present in the radar waveforms. Indeed, the freshwater ice signature depends on the properties and thickness of the snowpack and the ice layer and could be reduced or absent if some conditions are not met, as for instance in the case of snow-free lake ice or melting snow on the ice surface. In any case, the presence of the ice signature in the radar waveform is a requirement general enough to ensure the robustness of the method over a large number of freshwater lakes. Based on these findings, it can therefore be concluded that the LRM_LIT retracker method is a novel and promising tool for monitoring variability and trends in LIT.

4. Product Generation Based on Backscatter/Brightness Temperature and Validation (EOLA/LEGOS)

This section summarizes the LIT product generation with the empirical approach based on backscatter (Sig0) and brightness temperature (Tb) data. Details of the algorithm and its validation can be found in D2-ATBD document. Here the approach was developed and validated for both ENVISAT and Jason-2 data using Baker Lake, Great Slave Lake and Great Bear Lake (Keith Arm and McTavish Arm), Canada, as the target lakes.

The structure of LIT output product from the empirical method is presented in Table 2. Data is provided in csv format.

Table 2. List of LIT product variables

Variable name	Description	Units	Type	Dims
time	Time of measurement	decimal year	do	time
year	year of measurement		do	time
month	month of measurement		do	time
day	day of measurement		do	time
lon	Lake center longitude [-180;+180]	degrees	do	time
lat	Lake center latitude [-90;+90]	degrees	do	time
LIT_sigKu	Ice thickness retrieved from Ku backscatter by empirical method [0; 3]	m	do	time
LIT_tb18	Ice thickness retrieved from brightness temperature measurements in 18GHz frequencies by empirical method [0; 3]	m	do	time
LIT_avr	Ice thickness obtained by averaging of LIT_sigKu and LIT_tb18, [0; 3]. Allows for compensation of LIT_sigKu and LIT_tb18 outliers in pre-melting period.	m	do	time
LIT_sigKu_std	Standard deviation of Ice thickness retrieved from Ku backscatter by empirical method for a given date [0; 3]	m	do	time
LIT_tb18_std	Standard deviation of Ice thickness retrieved from brightness temperature measurements in 18GHz frequencies by empirical method for a given date [0; 3]	m	do	time
Lit_avr_std	Standard deviation of Ice thickness obtained by averaging of LIT_sigKu and LIT_tb18, [0; 3].	m	do	time
mission	Satellite mission name used for LIT retrievals		char	time
Flag	LIT retrieval quality flag [0,1,2,3]		int	time

4.1. Product Generation

4.1.1. Input Data

The following satellite products and model simulations are used for the product generation:

1. GDR product of ENVISAT on main orbit (2002-2010).
2. GDR product of ENVISAT on derivate orbit (2011-2012).
3. GDR product of Jason-2 on main orbit (2008-2016).
4. MODIS Terra, MODIS Aqua RGB images (2002-2016) available from NASA at <https://worldview.earthdata.nasa.gov/>
5. Ice thickness simulations generated from CLIMo model (Duguay et al., 2003) runs with 15 configurations for Great Slave and Baker Lake and 10 configurations for the Great Bear Lake (2008-2016).

4.1.2. Method

Step 1. Extraction of altimeter and radiometer measurements within a region with more or less homogeneous ice structure/snow regime. For each cycle, the measurements are averaged within a region to produce SigKu and Tb time series. One region was selected on both Great Slave and Baker lakes and two regions - with snow (Keith Arm) and with low snow cover (McTavish Arm) - on Great Bear Lake. For enhancing the temporal frequency of the ENVISAT LIT product, the Region of Interest (ROI) on each lake covers several ENVISAT tracks. This produces noise on the time series. Before processing, the time series were smoothed with a LOESS filter. The filtering allowed for reduction of the effect of ice metamorphism in the pre-melt period (resulting in a drop of Sig0 up to 10 dB) on the LIT retrievals as well.

Step 2. Definition of ice presence is based on Sig0Ku-Tb/2 algorithms tuned for each lake. The algorithm does not handle well the period of thermal degradation of ice during spring melt. For correction, two additional algorithms based on temporal variation of Tb24 (ENVISAT) or Tb18 (Jason-2) and on the difference Tb37-Tb24 (or Tb34-Tb18) (Zakharova et al., 2021) were applied.

Step 3. Satellite SigKu and Tb18/24 time series were divided into calibration (2008-2010 for ENVISAT and 2008-2012 for Jason2) and validation periods (2011-2012 for ENVISAT and 2013-2016 for Jason2). Relations between CLIMo-derived LIT and satellite backscatter/brightness temperature measurements were fitted with polynomial functions of degree 2, 3 or 4 depending on lake. A polynomial function of low degree (2) is better adapted for retrieving the maximum seasonal LIT, however, it produces more outliers during pre-melt and melt periods. Polynomial functions of degree 3 or 4 better handle LIT retrievals during ice metamorphism and decay. However, in this case the retrievals of maximum seasonal LIT are underestimated, especially for cold years.

Calibration was run with each CLIMo LIT configuration. A cost function built on the correlation (R), RMSE and Bias statistics calculated between modelled and altimetric LIT for the calibration period, was used for selection of model configuration, which better match altimetric LIT retrievals. As a result, the following model configurations were selected for calibration and validation of LIT: 0%Snow/30m mixing depth for the Baker Lake, 50%Snow/40m mixing depth for the Great Slave Lake and 75%Snow/40m mixing depth for the Great Bear Lake. 0% snow corresponds to no snow on the ice surface while 50% and 75% correspond to half and three quarter of the snow that is measured at a nearby meteorological station on land, respectively - knowing that less snow accumulates on the open ice surface of large lakes due to redistribution/packing by wind compared to a land surface.

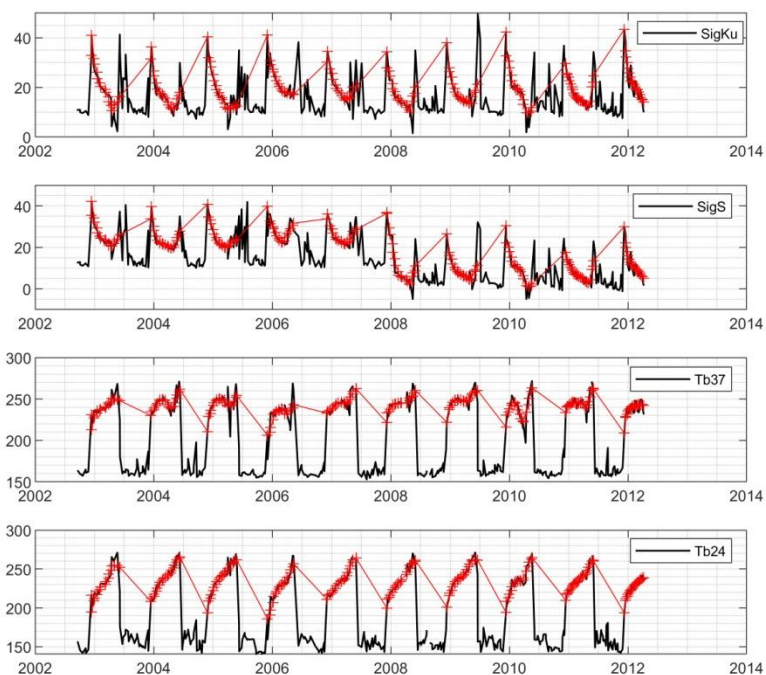


Figure 8. ENVISAT time series of SigKu, SigS, Tb37 and Tb24 extracted for Great Slave Lake. Measurements corresponding to the ice period selected for LIT retrievals are shown by red crosses. Note that backscatter generally decreases while brightness temperature increases during ice seasons, associated with ice growth.

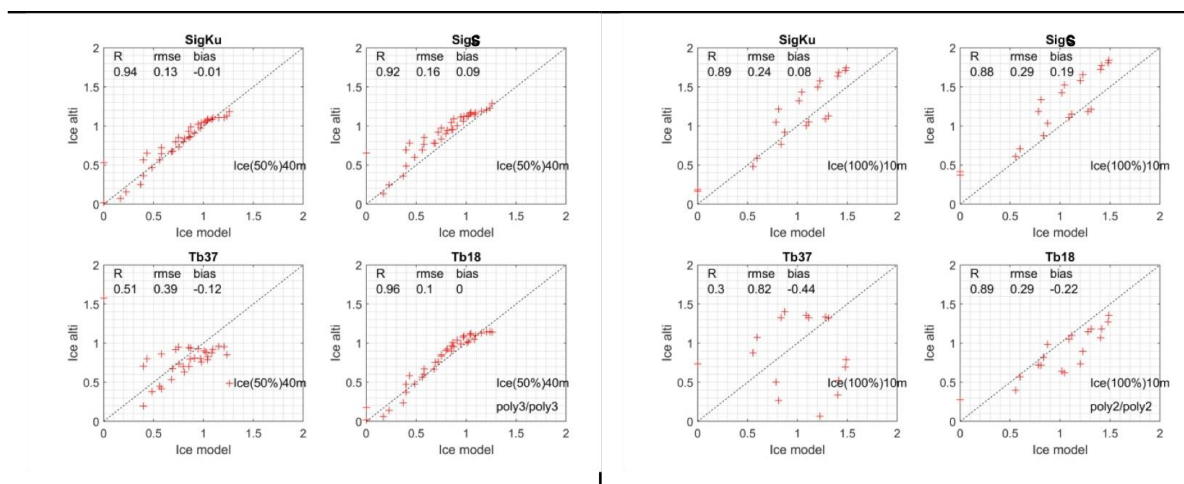


Figure 9. Scatterplot of LIT retrieved from ENVISAT altimetry and simulated by CLIMO for Great Slave Lake (left panel) and Baker Lake (right panel). CLIMO configurations and order of SigO/Tb fitting functions used are shown on each graph. LIT retrievals from SigS and Tb37 are also presented.

4.2. Validation

For validation, the correlation coefficient (R), RMSE and Bias statistics estimated over initial LIT retrievals (outliers included) were used. In many cases, LIT retrievals based on SigKu measurements overestimate LIT simulated by the CLIMO, while those based on Tb underestimate modeled LIT. The

average from these LIT_SigKu and LIT_Tb18/24 produced better validation scores for Baker Lake and Great Slave Lake (Figure 10 and Table 3). Snow-on-ice conditions on Great Bear Lake express high spatial and inter-annual variability likely due to the redistribution of snow by wind. This strongly affects the radar measurements and results in low accuracy of the LIT_SigKu retrievals using ENVISAT radar altimeter measurements. The low number of ENVISAT measurements available for calibration due to the 35-day repeat cycle (30 points) also has a negative influence on the LIT retrievals under these variable surface conditions. Moreover, to obtain this more or less adequate number of points for calibration and validation periods, large ROIs included at least two ENVISAT tracks for each lake. Differences in ice surface conditions between the two tracks on the Great Bear Lake could also introduce higher uncertainties in the ENVISAT LIT retrievals.

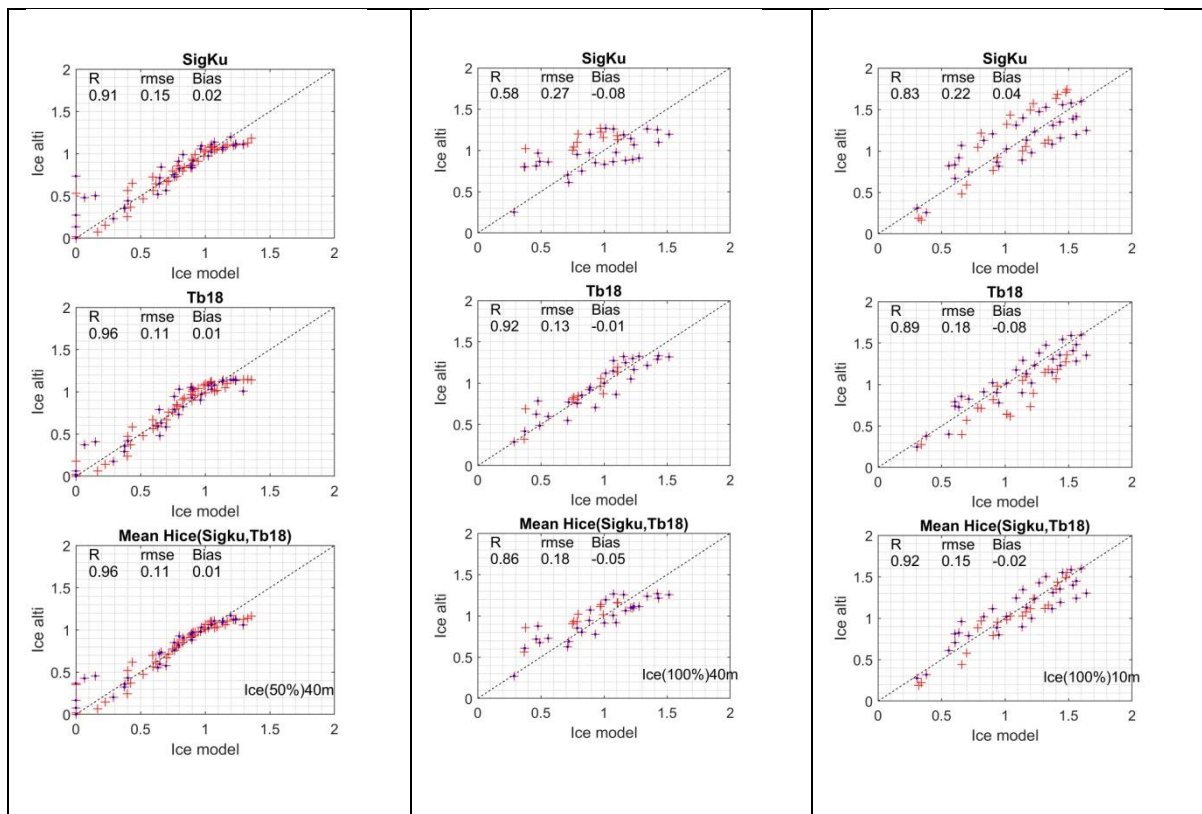
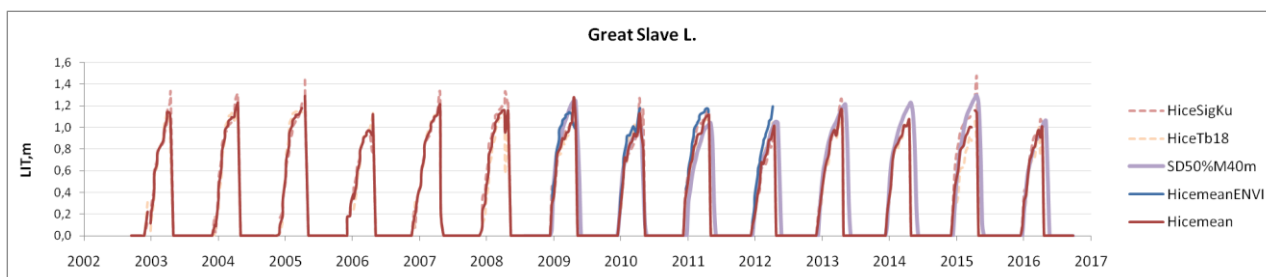
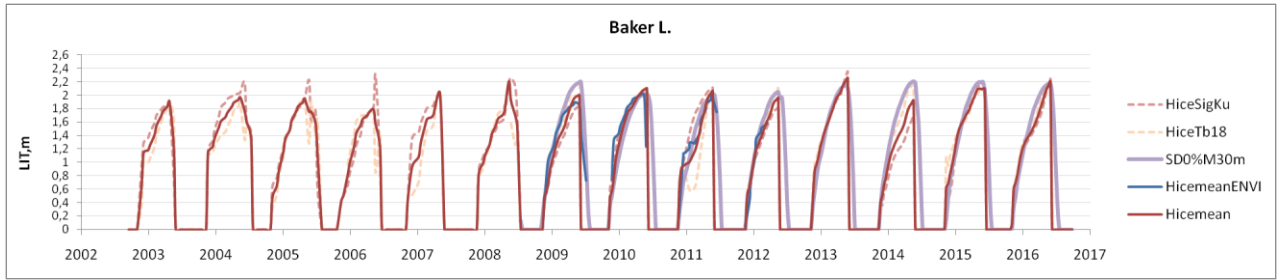


Figure 10. Scatterplot of LIT retrieved from ENVISAT altimetry and simulated by CLIMO for Great Slave Lake (left panel), Great Bear Lake -McTavish (center panel), and Baker Lake (right panel). CLIMO configurations used are shown at the bottom of individual plots. Measurements used for calibration are highlighted by blue points. Statistics (R, rmse, Bias) shown on the plots were calculated for all (calibration + validation) periods.

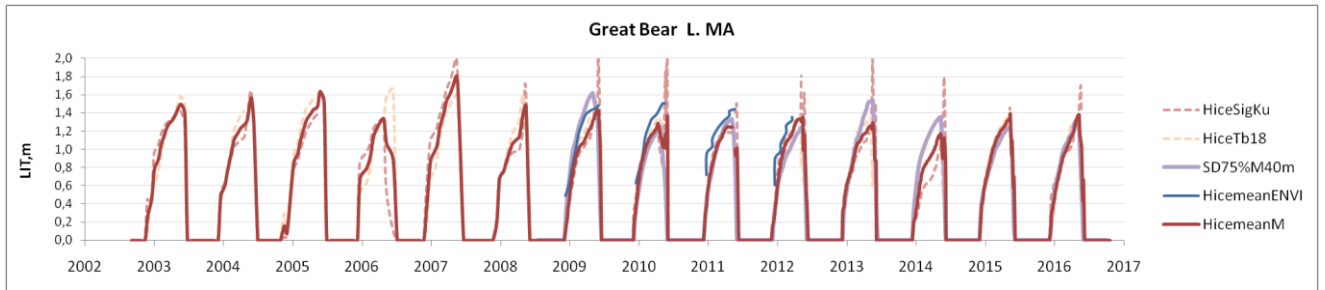


a)

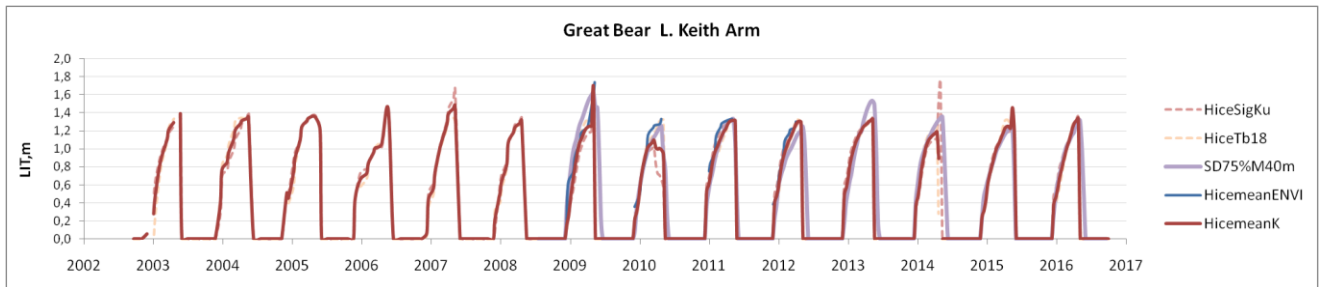
D4-2: Product Generation and Validation



b)



c)



d)

Figure 11. LIT retrievals for a) Great Slave Lake, b) Baker Lake, c) Great Bear Lake (McTavish Arm), and d) Great Bear Lake (Keith Arm) from ENVISAT and Jason-2 measurements compared to LIT CLIMo simulations (purple). ENVISAT LIT retrievals from ENVISAT and Jason-2 common period are shown in blue.

Table 3. Scores for LIT retrievals from ENVISAT and Jason-2 measurements for validation period.

Lake/validation period		ENVISAT (2011-2012)			Jason-2 (2013-2016)		
		LIT_SigKu	LIT_Tb18	LIT_avr	LIT_SigKu	LIT_Tb18	LIT_avr
Baker	R	0.89	0.89	0.97	0.91	0.94	0.95
	RMSE	0.24	0.29	0.11	0.29	0.20	0.20
	Bias	0.08	-0.22	-0.05	-0.16	-0.01	-0.08
	Nobs	20	20	20	74	74	74
Great Slave	R	0.63	0.85	0.76	0.94	0.95	0.97
	RMSE	0.24	0.16	0.19	0.12	0.16	0.11
	Bias	-0.01	-0.05	-0.03	0.01	-0.11	-0.05
	Nobs	42	42	42	62	62	62
Great Bear (Keith Arm)	R	0.37	0.98	0.85	0.95	0.96	0.97
	RMSE	0.30	0.20	0.30	0.13	0.11	0.1
	Bias	0.13	0.15	0.21	0.02	0.02	0.03
	Nobs	18	18	18	55	55	55
Great Bear (McTavish Arm)	R	0.79	0.90	0.90	0.76	0.94	0.88
	RMSE	0.33	0.11	0.20	0.28	0.15	0.18
	Bias	0.28	0.04	0.16	-0.11	0.02	-0.03
	Nobs	11	11	11	114	114	114

Considering the short validation period, the uncertainties of LIT time series retrieved from the empirical approach provided in the final product are calculated for the whole ENVISAT and Jason-2 operation periods, i.e. they include the calibration period as well (Table 4). The product also contains a flag [0,1,2,3] indicating a quality of retrievals. Flag=0 corresponds to ice-free period derived using Sig0Ku-Tb/2 approach for the end of open water period (see ATBD) and using optical MODIS RGB images for the end of "consolidated ice" period. Flag=1 indicates LIT retrievals with known uncertainties (Table 2). Flag=2 is attributed to LIT retrievals after the ice surface has undergone radiative metamorphism in the pre-melt period (Zakharova et al., 2021). These LIT retrievals are of unknown accuracy. Flag=3 indicates the dates of satellite lake overflight during the ice period, when LIT retrievals were out of physical range [0 3 m] (mostly during spring and summer when radar and radiometer signals are affected by water-on-ice).

Table 4. Scores for LIT retrievals from ENVISAT and Jason-2 measurements for the whole (calibration and validation combined) period.

Lake/validation period		ENVISAT (2008-2012)			Jason-2 (2008-2016)		
		LIT_SigKu	LIT_Tb18	LIT_avr	LIT_SigKu	LIT_Tb18	LIT_avr
Baker	R	0.80	0.88	0.89	0.89	0.93	0.95
	RMSE	0.34	0.27	0.23	0.27	0.22	0.18
	Bias	0.07	-0.09	-0.02	-0.07	-0.02	-0.05
	Nobs	52	50	49	159	158	158
Great Slave	R	0.92	0.88	0.94	0.88	0.92	0.94
	RMSE	0.13	0.15	0.11	0.16	0.14	0.12
	Bias	0.00	-0.03	-0.01	0.03	-0.05	-0.01
	Nobs	84	84	84	103	102	101
Great Bear (Keith Arm)	R	0.24	0.92	0.86	0.85	0.89	0.91
	RMSE	0.51	0.15	0.18	0.18	0.16	0.14
	Bias	0.14	0.04	0.02	-0.01	-0.02	-0.02
	Nobs	47	41	41	117	116	116
Great Bear (McTavish Arm)	R	0.36	0.75	0.64	0.79	0.95	0.91
	RMSE	0.43	0.26	0.32	0.23	0.12	0.15
	Bias	0.26	0.10	0.18	-0.08	0.00	-0.04
	Nobs	45	44	44	246	247	246

4.3. Conclusion and Recommendations

The empirical approach provides a good precision of LIT retrievals for Great Slave Lake and Baker Lake. The retrievals are of higher uncertainties for the Great Bear Lake likely due to high short-term and interannual variability of ice surface conditions. The use of average LIT retrieved from backscatter and brightness temperature measurements is preferred for Great Slave and Baker lakes. For Great Bear Lake, the LIT retrievals from brightness temperature measurements alone should be privileged.

Better detection of melt onset could be beneficial for LIT retrievals from empirical equations. A combination with the CCI_Lakes Lake Ice Cover (LIC) product could be envisaged for improving the quality flags.

At present, the obtained LIT-Sig0 or LIT-Tb relations are lake and satellite specific. The creation of a general relation independent of lake snow conditions, ice texture and radar parameters is of great interest. Based on results of LIT retrievals over the Ob River using Jason-2 altimeter measurements (Zakharova et al., 2021), a test of predictive efficiency of derivative of Sig0 and Tb was performed for the Great Slave Lake. For retrieving the ice thickness on the Ob River, a cumulative difference obtained from consecutive satellite cycles measurements of Sig0 or Tb (CDif_Sig or CDif_Tb) was used instead of absolute values of Sig0 and Tb.

A comparison of LIT retrieved from Jason-2 CDif_Sig or CDif_Tb parameters and equations developed for ENVISAT (ENVISAT coefficients applied to Jason-2 CDif_Sig or CDif_Tb), demonstrate that using the cumulative difference the inter-mission/inter-instrument biases likely could be neglected.

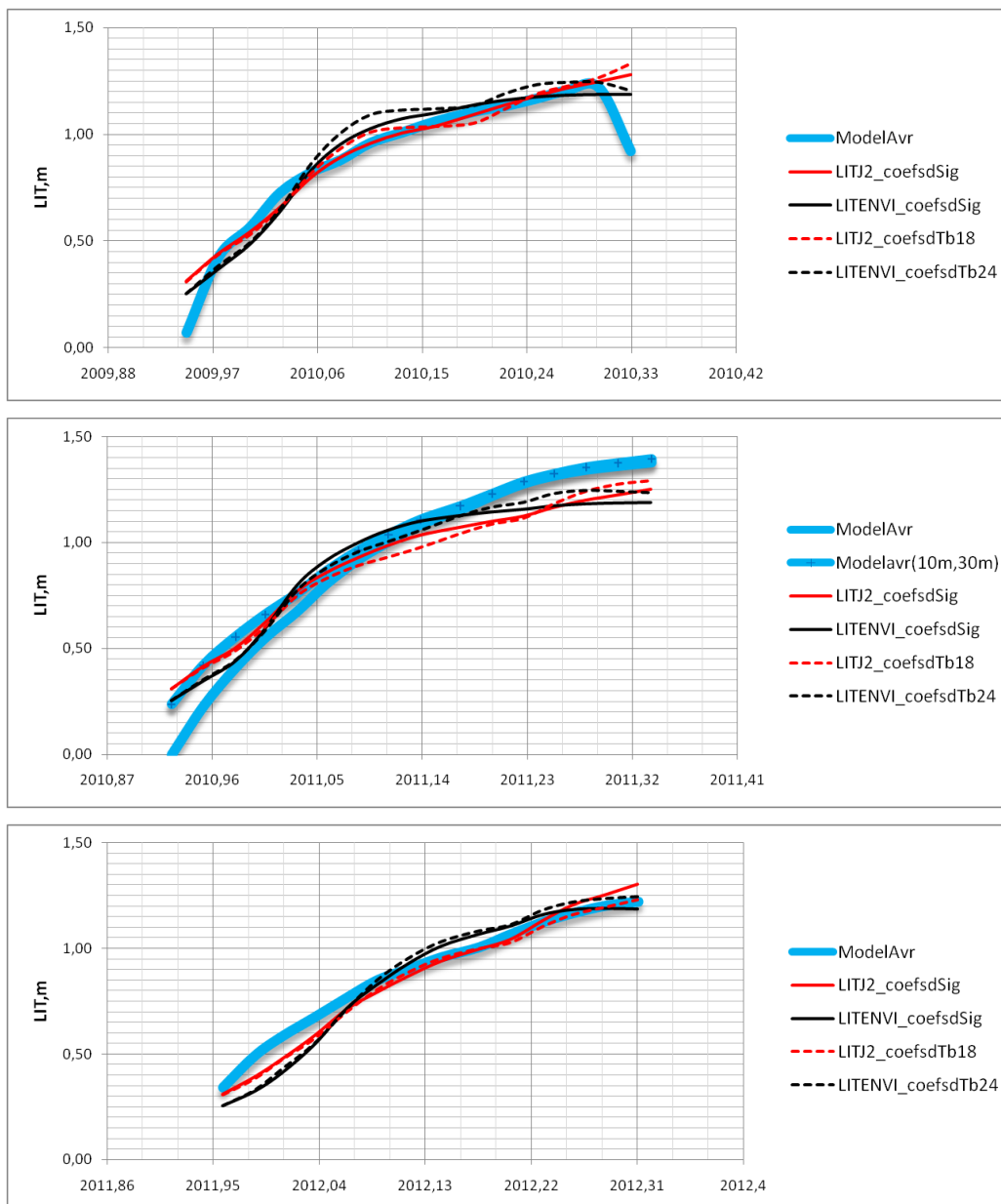


Figure 12. Great Slave Lake LIT retrievals for winters 2010, 2011 and 2012 using Jason-2 CDifSig and CDifTb with equation parameters obtained for Jason-2 (red lines) and ENVISAT (black line) missions. Modeled LIT represent an average from CLIMo configurations "100%snow/30m". For 2011 CLIMo LIT average from "10m-30m" mixing depth configurations is also shown.

One inconvenience of the CDif_Sig/Tb method relates to its dependency on initial conditions. If the ice onset was missed or Sig0/Tb values were exceptionally low/high at the ice onset, the LIT retrievals become highly underestimated (see 2015 on Figure 13). According to MODIS images, in November-December 2014, ice in the ROI of Great Slave Lake was already covered by snow in contrast to other years. As a result, Sig0 at the ice onset was significantly lower compared to previous years (Figure 14), when the black (snow-free) ice was visible on MODIS images until January.

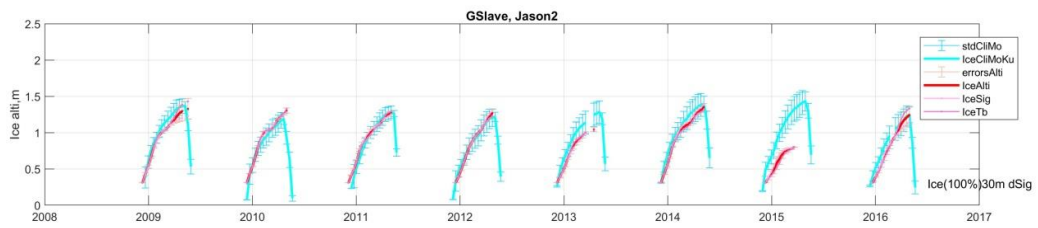


Figure 13. LIT retrievals for Great Slave Lake from Jason-2 measurements compared to LIT CLIMo simulations with configuration 100%snow30m mixing depth based on the cumulative difference approach. CLIMo LIT variability due to different model configurations adjacent to the selected one is shown as error bars.

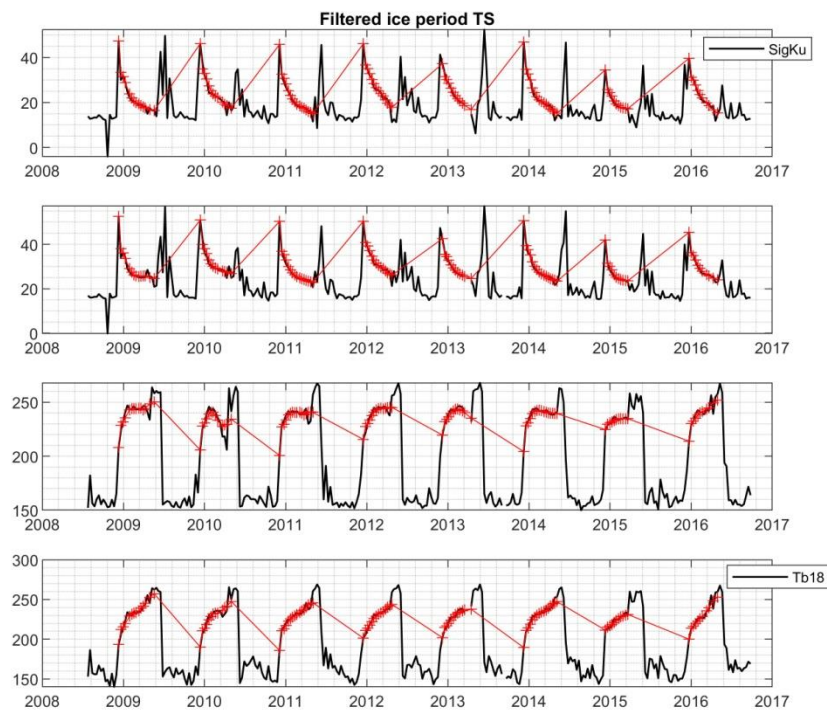


Figure 14. Jason-2 time series of (from top to bottom) SigKu, SigC, Tb24 and Tb18 extracted for Great Slave Lake. Measurements corresponding to ice period selected for LIT retrievals are shown by red crosses.

The approach based on Sig0 or Tb derivatives will likely allow the unification of empirical equations in future, but this will require a follow-up investigation for determination of its benefit and limitations.

5. Comparison of LIT Retrievals from Radar Waveforms and Backscatter/Brightness Temperature Approaches

A comparison of LIT estimates obtained from the analytical and empirical approaches was possible at Great Slave Lake using Jason-2 (track 45) data acquired for three overlapping ice seasons (2013-2014, 2014-2015, and 2015-2016). It is worth noting that in situ measurements of LIT are available for the lake but they are collected in a bay near the shore, some 70 km away from the area of track 45 analyzed herein (see Figures 1 and 7). The depth of snow on the ice surface may be very different near the shore compared to the more open area at the centre of Great Slave due to the redistribution of snow by wind. Hence, the thermodynamic lake ice model CLIMo was used for algorithm calibration and validation in the empirical approach (details in section 4), while it is also used for validation of the analytical approach (details in section 3) for the area of interest near the centre of Great Slave Lake.

Based on the analytical approach (Mangilli et al., 2022), the MBE and RMSE between Jason-2 and CLIMo (25% snow scenario) in the middle of the ice season for ice season 2013-2014 are 0.073 m and 0.077 m, respectively. These results are in line with expectations, as the winter was colder over the study area during that winter, with less snow than the two other years. For the 2014-2015 ice season, the Jason-2 LIT estimates are in good agreement with the thermodynamics simulations with a 70% snow on ice scenario as input, in particular in the middle of the ice season, where the MBE and the RMSE between the two data sets is of 0.025 m and 0.044 m, respectively. Jason-2 LIT are also in strong agreement with CLIMo simulations with 50% of snow on ice as input, where the MBE is 0.002 m and the RMSE is 0.019 m.

In the case of the empirical approach which uses a constant on-ice snow scenario of 50% in each ice season (2013-2016), errors in Jason-2 LIT estimates are RMSE of 0.12 m (SigKu), 0.16 m (Tb18) and 0.11 m (average SigKu and Tb18) and bias of 0.01 m (SigKu), -0.11 m (Tb18) and -0.05 m (average SigKu and Tb18). RMSE values are smallest when LIT estimates from backscatter (Ku-band) and Tb (18 GHz) are combined into an average. However, it should be noted that by doing this, the estimated LIT represents a larger area from track 45 since the footprint of the passive microwave radiometer is in the order of a few tens of km rather than ca. 5-6 km when Ku-band radar altimeter data is used alone.

Plots provided in Figure 15 illustrate the seasonal evolution of LIT estimated from the two approaches for the overlapping ice seasons (2013-2016). Both approaches provide LIT values that follow the expected temporal trajectory of ice thickening from initial ice formation to melt onset. While there is relatively good agreement in the middle of the ice season (late January to mid-April) in 2014-2015 and 2015-2016 (LIT differences of ca. 0.10 m on average), large discrepancies (0.30-0.50 m) are revealed during the 2013-2014 ice season as well as at the beginning of ice formation (as much as 0.30 m) and at or near the onset of melt. This can partly be attributed to the fact that the empirical approach uses an average value of 50% snow on ice regardless of ice season. It has been shown that the percentage of snow on ice compared to that of land (the reference for calculating the percentage of snow on ice) varies from year-to-year on Great Slave Lake and, after air temperature, is the most important driver of ice growth (Kheyrollah Pour et al., 2017). On the other hand, the analytical approach estimates LIT based on reflections of the radar signal from the snow-ice and ice-water interfaces such that variations in snow on ice are somewhat captured. Finally, the two approaches provide widely different LIT estimates at or near the melt period in April, in the order of 1.00-1.50 m. The empirical approach always detects ice melt onset (LIT of 0.00 m) one cycle (10 days) ahead of the analytical approach (LIT of 1.17 to 1.57 m depending on ice season). The discrepancy may be related to the efficiency of each approach in detecting the beginning of melt. Further work (several years and missions) is needed to fully assess this.

D4-2: Product Generation and Validation

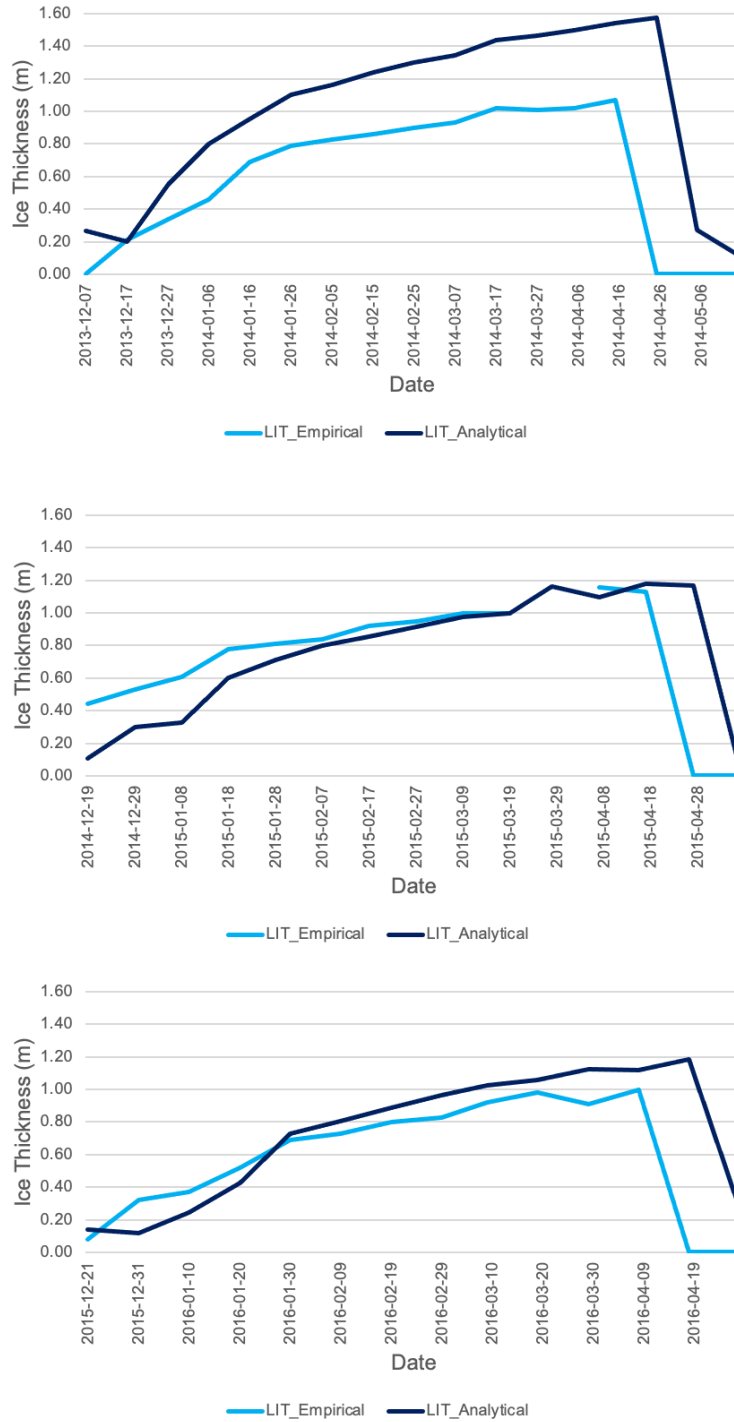


Figure 15. Comparison of LIT retrievals between the analytical and empirical approaches for ice seasons 2013-2014 (top), 2014-2015 (middle) and 2015-2016 (bottom) from Jason-2 data (track 45) at Great Slave Lake. LIT from the empirical approach is the average value calculated from Ku-band backscatter and T_b at 18 GHz.

6. References

Duguay, C.R., G.M. Flato, M.O. Jeffries, P. Ménard, K. Morris, and W.R. Rouse, 2003. Ice cover variability on shallow lakes at high latitudes: Model simulations and observations. *Hydrological Processes*, 17(17): 3465-3483.

Kheyrollah Pour, H., C.R. Duguay, A. Scott, and K.-K. Kang, 2017. Improvement of lake ice thickness retrieval from MODIS satellite data using a thermodynamic model. *IEEE Transactions on Geoscience and Remote Sensing*, 55(10): 5956-5965, doi: 10.1109/TGRS.2017.2718533

Mangilli, A., P. Thibaut, C.R. Duguay, and J. Murfitt, 2022. A new approach for the estimation of lake ice thickness from conventional radar altimetry. *IEEE Transactions on Geoscience and Remote Sensing*, 10.1109/TGRS.2022.3186253 (Early view - 24 June 2022).

Zakharova, E., S. Agafonova, C. Duguay, N. Frolova, and A. Kouraev, 2021. River ice phenology and thickness from satellite altimetry. Potential for climate studies and ice bridge road operation. *The Cryosphere*, 15: 5387-5407, <https://doi.org/10.5194/tc-15-5387-2021>.